Vibration response demodulation, shock model and time tracking

Xavier Laval, Nadine Martin, Pascal Bellemain, Z y Li, Corinne Mailhes, Christian Pachaud

Vibration response demodulation, shock model and time tracking

Journal:	*CM 2018 and MFPT 2018*
Manuscript ID	Draft
Topic:	Condition monitoring (CM) methods and technologies
Date Submitted by the Author:	n/a
Complete List of Authors:	Martin, Nadine; GIPSA-lab, Grenoble campus,
Keywords:	Vibration analysis, Signal processing, Demodulation, Hilbert transform, Signal model

Vibration response demodulation, shock model and time tracking

X. Laval, N. Martin, P. Bellemain, Z. Y. Li
Univ. Grenoble Alpes, CNRS, Grenoble INP*, GIPSA-Lab, 38000 Grenoble, France
* Institute of Engineering Univ. Grenoble Alpes
+33 4 76 57 47 16
xavier.laval@gipsa-lab.grenoble-inp.fr

C. Mailhes
Univ. of Toulouse, IRIT/INPT-ENSEEIHT /TéSA, 31000 Toulouse, France

C. Pachaud
Senior technical consultant, 3 place Sadi Carnot 87350 Panazol, France

Abstract

A reliable monitoring of a rotating machine needs amplitude and phase demodulation over well-chosen frequency bands. Although often applied, the behaviour of this estimator is not so well established in such a context and particularly for earlier and accurate fault detection. In attempt to provide keys for the understanding of vibration measures, this paper proposes a vibration signal model of a faulty gearbox. More attention is given to the amplitude modulation function to better model the shocks created by local tooth defects and incurred by all the meshing frequency harmonics. The proposed shock model is defined as the response of a mechanical system excited by a Dirac function assuming that the fault does not evolve during the measure. Parameters of resulting response models, exponentially periodic waves, are set to fit as much as possible to a sequence of signals to model the time evolution of the GOTIX bench during a fatigue test. All signals are processed by AStrion, an automatic and data-driven spectral monitoring approach. Interestingly, setting various fault model parameters, damping factors, amplitude modulation rates, frequency modulation indexes, fault location and number, helps for the understanding of the modulation phenomenon and illustrates the intrinsic limits of the demodulation approach.

1. Introduction

The preventive maintenance of a complex system including several rotating machines needs the use of advanced signal processing tools for early and accurate fault detection. Moreover, for an offline continuous monitoring, a sequence of data should be analysed and tracked automatically. In this context, this paper proposes to study one particular step of this analysis. After peak detection, harmonic family and sideband classification, tracking of associated features, the diagnosis is completed with a fault characterisation that can be achieved thanks to a demodulation process. This paper focusses on the classical approach by band pass filtering and Hilbert transform. This method can perform well provided that some constraints are satisfied. In attempt to provide keys for the understanding of vibration measures, this paper proposes the parallel analysis of real-world signals measured on the test bench GOTIX, and vibration signal models of the same gearbox. More attention is given to the amplitude modulation function to

better model the shocks created by local tooth defects and incurred by all the meshing frequency harmonics. This study supports the development of AStrion, a tool dedicated to automatic and data-driven analysis. Section 2 briefly recalls the AStrion concept. Section 3 derives the vibration model of a faulty gearbox. Sections 4 and 5 propose respectively frequency and amplitude modulation function models in the case of a local fault on a gear tooth. Section 6 examines the demodulation of signals generated from the models versus a real-world measure in order to justify the model choices. Then the limits of the Hilbert demodulation are underlined in Section 7. Section 8 draws the conclusions and perspectives.

2. Continuous monitoring and the demodulation phase

For a continuous and automatic monitoring, AStrion is a data-driven tool including a set of modules from data validation, to peak, harmonic-sideband detection[(1)] and creation of a wide list of advanced features, or fault indicators, that can be *a posteriori* associated to kinematic values of the system analysed. For surveillance, a dedicated time-frequency tracking over all previous timestamps[(2)] builds trajectories of peak, harmonic and sideband families that generate continuous system health indicators. This approach has been validated on onshore wind turbines[(3)(4)(5)] and paper machines[(6)].

One of the AStrion modules, called AStrion-M[(7)], gives the possibility to demodulate any frequency band containing the detected side bands around one detected carrier. This paper aims at assessing this module through the investigation of a vibration signal model. The background of the method is very classical, namely a band pass filtering, followed by a time synchronous averaging, amplitude and phase/frequency modulation function estimations after a Hilbert transform. The innovative part of AStrion applies a multi-rate filtering which design is data-driven and fully automatic whatever the size of the spectral band, also automatically set by the previous modules of AStrion. The multi-rate filtering is a solution for having stable filters.

In a nutshell, the method is derived in an iterative process driven by a filter stability criterion. If the band-pass filter with the given spectral band is stable, the band-pass filtering is applied, the frequency shifting is done in one go, the signal is then down-sampled and demodulated. The chosen band-pass filter is an elliptic one, a sharp roll-off being required. If not, if the high pass filter from the lower frequency boundary of the given spectral band until the Shannon frequency is stable, this high-pass filtering is applied followed by iterations of low-pass filtering and down-sampling, with a final demodulation. The chosen high-pass filter is an elliptic one also. The low-pass filter is a Butterworth one. If both filters are unstable, a sequence of decimation (low-pass filter and down-sample) is iterated until the band-pass of high-pass filter is stable.

The inputs of AStrion-M are the outputs of the harmonic and side band detection, namely AStrion-H. Before the filtering step of AStrion-M is applied a time synchronous averaging with the fault frequency. The outputs of each AStrion-M demodulation are then the amplitude and phase/frequency demodulation functions in angle on one rotation of the faulty component and a list of indicators. In a continuous monitoring, the indicators are associated between the different time stamps. This tracking is of interest to evaluate the evolution of the state of the system.

Even though other demodulation approaches exist, this paper will focus on this Hilbert approach only in order to highlight and illustrate two problems, the filter band sensitivity and the Bedrosian constraints on the amplitude demodulation function versus

the phase demodulation function[12] depending on the model proposed and its parameters.

3. Vibration signal model of a faulty gearbox

This paper will consider a pair of meshing gears at steady-state conditions, so with mesh under a constant speed and load. Such a healthy system at nominal speed and at a given load produces a vibration component due to the transmission error of each pair of the meshing gears. This component, due to the elastic deformation of the loaded teeth, is load dependent and periodic of the gear mesh frequency with integer harmonics. In addition, geometrical deviations from the ideal tooth profiles, intentional or unintentional, contribute also to the error transmission but is non-load dependent. Moreover the meshing force has also reactions in the shafts that support the gear. It causes vibration components at both the gear and pinion frequencies at a smaller amplitude level but with also a number of harmonics. In this paper the reaction of the shafting bearings is not considered. In case of a healthy system, a signal vibration model denoted as $x_{healthy}(t)$ can be written as

$$x_{healthy}(t) = \sum_{h=1}^{N_H} A_h^{mesh} \sin\left(2\pi h f^{mesh} t + \phi_h^{mesh}\right) + \sum_{r=1}^{N_G} A_r^{gear} sin\left(2\pi r f^{gear} t + \phi_r^{gear}\right) + \sum_{p=1}^{N_P} A_p^{pinion} \sin\left(2\pi p f^{pinion} t + \phi_p^{pinion}\right) + \mathrm{n}(t), \quad (1)$$

where, for the gear mesh frequency f^{mesh}, N_H is the harmonic number, A_h^{mesh} the amplitude and ϕ_h^{mesh} the phase of the h^{th} harmonic, for the gear shaft frequency f^{gear}, N_G is the harmonic number, A_r^{gear} the amplitude and ϕ_r^{gear} the phase of the r^{th} harmonic, for the pinion shaft frequency f^{pinion}, N_P is the harmonic number, A_p^{pinion} the amplitude and ϕ_p^{pinion} the phase of the p^{th} harmonic. In addition of these deterministic parts induced mainly by the meshing force, the random part of the vibration signal and the non-periodic components n(t) are simply approximated here by a stationary Gaussian white noise.

Let it now assume a local defect on the gear such as a flaking which produces one impact each gear rotation. This impact or shock induces fluctuations in the torque transmitted by the gears. These dynamic transmission errors induce phase modulations when the motor is asynchronous and amplitude modulations due to the variations of the meshing force. The measured signal is then modulated in amplitude and phase by functions periodic with the rotation frequency of the shaft supporting the faulty gear. Therefore, the signal vibration model in Eq. (1) denoted now as $x_{faulty}(t)$ is modified as

$$x_{faulty}(t) = \sum_{h=1}^{N_H} \mathrm{AM}_h(t) \sin\left(2\pi h f^{mesh} t + PM_h(t) + \phi_h^{mesh}\right) + \sum_{r=1}^{N_G} A_r^{gear} sin\left(2\pi r f^{gear} t + \phi_r^{gear}\right) + \sum_{p=1}^{N_P} A_p^{pinion} \sin\left(2\pi p f^{pinion} t + \phi_p^{pinion}\right) + \mathrm{n}(t), \quad (2)$$

where $AM_h(t)$ and $PM_h(t)$ are the amplitude and phase modulation function of the h^{th} harmonic of f^{mesh} respectively. The phase relationships of the sidebands on either side of f^{mesh} are different between the amplitude and phase modulations. All these vibration sources are transmitted via a transmission path through the structure to the point

measurement where the accelerometer is located. The measure is then the result of a convolution with the impulse response of the transmission path. Unfortunately, the vibration signal after the transfer function of the structure can be a mix of these demodulations and lose this phase property[9]. This issue is not considered in this paper.

4. Frequency modulation function model

If we assume that a local fault is on the gear tooth, $PM_h(t)$ in Eq. (2) can be modelled with a sum of harmonic sine functions to the fundamental f^{gear}

$$PM_h(t) = \sum_{k=1}^{K} \beta_h^k sin(2\pi k f^{gear} t), \quad (3)$$

with β_h^k the frequency modulation index of the harmonic k of the fault frequency f^{gear}. The frequency excursion of harmonic k is equal to $2\beta_h^k k f^{gear}$. With Z_g the gear tooth number (see Appendix), the frequency modulation rate associated to order k of f^{gear} and order h of f^{mesh} is denoted FMR_h^k and defined as,

$$FMR_h^k = \frac{2\beta_h^k k f^{gear}}{2h f^{mesh}} = \frac{k\beta_h^k}{hZ_g}, \quad (4)$$

5. Amplitude modulation function model

5.1. As a discrete Fourier series

As the modulation is a periodic process, the modulation function is often represented by discrete Fourier series[10],

$$AM_h(t) = A_h^{mesh}\left(1 + \sum_{\ell=1}^{L} m_h^{\ell} sin(2\pi \ell f^{gear} t + \emptyset_h)\right), \quad (5)$$

with L the harmonic number, m_h^{ℓ} the amplitude modulation index of harmonic of order ℓ, $m_h^{\ell} \leq 1$, $\emptyset_h$ a random phase. All periodic function with a finite power can be decomposed in an infinite sum of sines, which argues for the use of this model. Nevertheless, the sinusoidal property of $AM_h(t)$ has no link with the physics, so the need for a high number L of modes. However, the high orders will be quickly embedded in the background and will have no influence in the model.
Moreover, this function can be negative. So, it is of great importance to add a positivity constraint to prohibit negative values which will induce higher harmonics in the amplitude and an additional phase term after demodulation. At some angles, the vibration amplitude of the faulty signal can be lower than the healthy vibration amplitude. As an alternative, the authors in[13] model the fault impact with a Hanning function, which length represents the angular duration of the impact.

5.2. As a shock response

To be closer to the physics and knowing that a local failure on a tooth generates shocks at each rotation, we propose to consider $AM_h(t)$ in Eq. (2) as the result of an impact or shock at each gear rotation. Let $t_{g\zeta}$ be the instant of the shock of the fault tooth ζ on a

rotation of the gear with regard to a tooth reference. We assume that the fault does not evolve during the measure so that $t_{g\zeta}$ is the same at each rotation. Each shock excites the resonance modes of the system which response is the sum of both the forced and free response of the system at these resonance modes. So for a measure over M rotations of the gear, a sequence of shocks occurs at $t_s^{\zeta} = t_{g\zeta} + s \times 1/f^{gear}$ with $\mathrm{s} = 1, \mathrm{M}$. The response of this multi-shock excitation is the sum of all the responses at these instants. If we define each shock as a Dirac function, this response can be written as

$$x_{faulty,fmesh}(t) = \sum_{h=1}^{N_H} A_h^{mesh} \sin\left(2\pi h f^{mesh} t + \phi_h^{mesh}\right)(t) + \sum_{s=0}^{M} \sum_{h=1}^{N_H} A_h^{mesh} m_h^s e^{-\alpha_h (t - t_s^{\zeta})} \, \mathrm{u}\left(t - t_s^{\zeta}\right) \sin\left(2\pi h f^{mesh} (t - t_s^{\zeta}) + \phi_h^{mesh}\right), \quad (6)$$

where $\mathrm{u}(t)$ is the Heaviside function. The damping factor α_h does not depend on the shock but on the system, so on index h only, and the amplitude m_h^s depends on both the forced and free response of the system excitation, so on both index s and h. More details are given in [8]. So $AM_h(t)$ writes as

$$AM_h(t) = A_h^{mesh} \left(1 + e^{-\alpha_h t} \, \mathrm{u}(t) * \sum_{s=0}^{M} m_h^s \, \delta\left(t - t_s^{\zeta}\right)\right), \quad (7)$$

the symbol $*$ denoting the convolution operation. In the following section, this model is tested by AStrion and compared to GOTIX test bench results.

6. Models versus real-world measures

GOTIX, a test bench located in GIPSA-lab to characterize defects on rotating machines is used to produce a database on a natural wearing of a gearbox with 2 parallel straight gears meshing together. The 2 gears are connected respectively to a driving asynchronous 3-phase motor rotating at 474 rpm and a loading DC-generator applying a 200Nm torque on the output shaft. The ratio between input and output shaft is 3.8. The detail of this bench can be found in appendix.

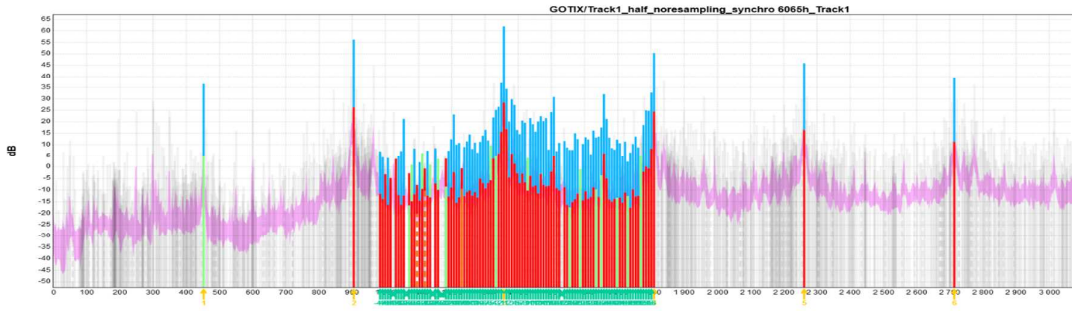

Figure 1: Spectral peaks detected by AStrion on a measured signal on GOTIX. Highlighted are the meshing harmonics with yellow arrows and the sidebands from the input shaft around the 3rd meshing harmonic with green arrows.

Figure 1 shows a healthy GOTIX signal with preponderant meshing harmonics modulated by both input and output shaft frequencies. From a signal of low to intermediate state of wear, AStrion provides the amplitude values of the peaks

associated to the harmonic families of input and output shafts, and gear mesh, thus providing the A_h^{mesh}, A_r^{gear}, A_p^{pinion} terms of equation (1). These values were used to generate simulated signals with the same pattern, thus simulating the healthy state of the gearbox. In order to create a faulty state, $AM_h(t)$ and $PM_h(t)$ have been added to these signals.
In a first study, Figure 2 shows $AM_h(t)$ modeled as described in section 5.1. Even if the positivity constraint is applied, the shape of a sine sum does not fit well with the estimated one from measured signals. Furthermore, choosing the parameters of this model is really a complex task if the number of faulty teeth and their location should be controlled.

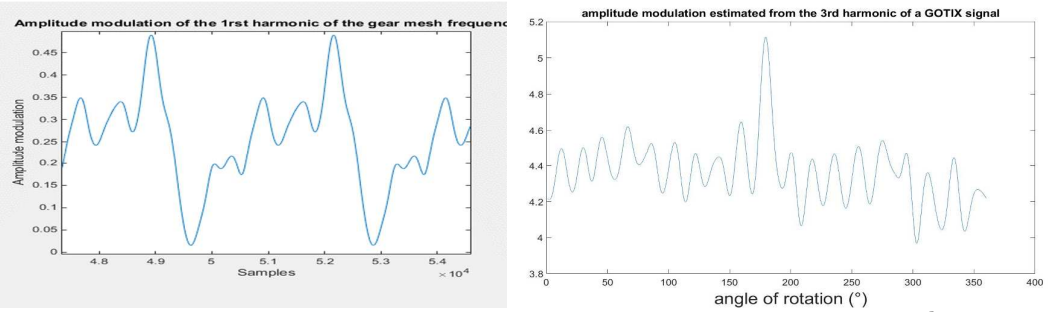

Figure 2: On the left, model of an $AM_h(t)$ of the first harmonic of f^{mesh} with 20 harmonic sines of the faulty frequency gear, a decreasing modulation index and a random phase, signal to noise ratio of 20 dB, duration 20 s. On the right, estimated $AM_h(t)$ of the 3rd harmonic of f^{mesh}in GOTIX test bench.

The estimated $AM_h(t)$ from GOTIX signal shows that, while most teeth generate amplitude variations of similar values, one generates a higher value. This is probably due to a fault on 1 tooth, and will be considered as a signature of a shock.

A second study have tested the proposed shock model of equation (6). The shock amplitude m_h^s is chosen constant at 3 in order to correspond to the estimated $AM_h(t)$ of the third harmonic of the GOTIX signal. This particular harmonic is chosen because of its highest energy, making the result clearer. In the simulated signals, this amplitude is constant for every harmonic. t^ζ is chosen as the instant of meshing of the 25th tooth.

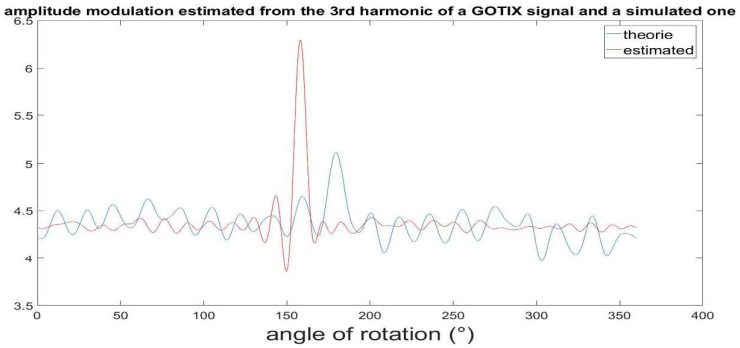

Figure 3: Estimated $AM_h(t)$ of the 3rd harmonic of a GOTIX signal (blue) and a simulated signal (red).

While the damping factor α_h is chosen constant for every harmonics in the same signal, five different values have been used to correspond to five different durations of the shock, from half a tooth to 8 teeth. The duration is calculated as the time for the shock to decrease to 5% of the initial value.

For a simulated signal with α_h corresponding to half a tooth and a GOTIX signal demodulated with the same bandwidth, **Figure 3** shows that $AM_h(t)$ parameters, especially the shock amplitude, are realistic considering that GOTIX is relatively healthy while the shock modulation aims to simulate a default on the gear.

Different $PM_h(t)$ have been tested:

- No $PM_h(t)$,
- $PM_h(t)$ as in equation (3), with *K=1* (1 sine) with different values of $\beta_h^k = c$ equal to 1, 5, 10 and 20 (same value for each harmonic),
- $PM_h(t)$ as in equation (3), with *K=4* where the dependence to the mesh harmonics is not taken into consideration, $\beta_h^k = \beta^k$ with β^k chosen to correspond to the estimated $PM_h(t)$ of the GOTIX signal. A multiplicative factor $c = 1, 5, 10$ and 20 is successively applied to β^k to simulate an increasingly faulty $PM_h(t)$. The comparison in Figure 4 shows that the actual GOTIX $PM_h(t)$ is more complicated, even though taking K=4 seems sufficient to have comparable amplitudes.

A noise has been added with a signal-to-noise ratio equivalent to the GOTIX measurements, estimated with AStrion[14].

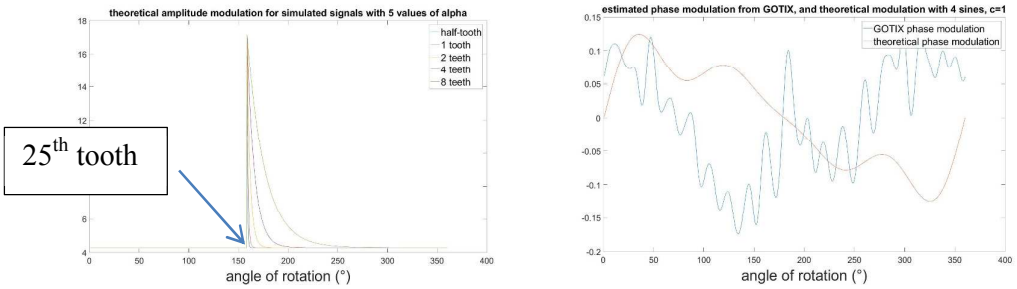

Figure 4: Theoretical $AM_h(t)$ with different damping factors (left) and $PM_h(t)$ with *K=4* (right) for one rotation with comparison with the GOTIX signal.

7. Limits of the Hilbert demodulation

7.1. Demodulation in a "friendly" case

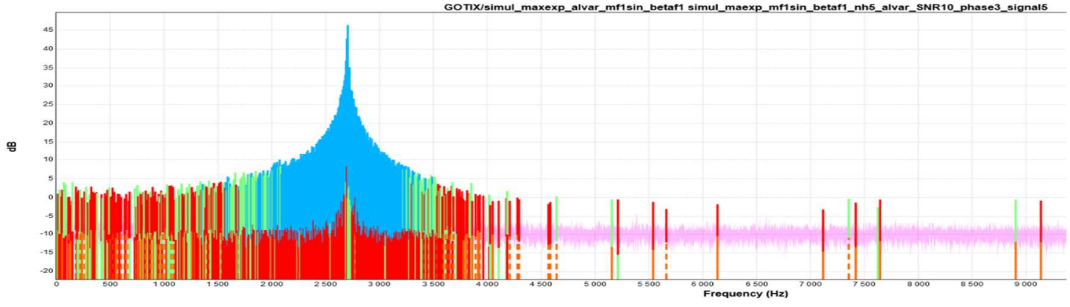

Figure 5: Spectral peaks detected by AStrion on the simulated signal with only one harmonic.

For a first evaluation of the performances of the demodulation method described in section 2, a simplified simulated signal has been considered with only the 6th harmonic of the mesh frequency in (2) to avoid interferences between harmonics and to have a great number of sidebands. As visible in the spectrum in Figure 5, the shock produces sidebands on a very large band. Thus, the demodulation has been performed on the whole spectrum.

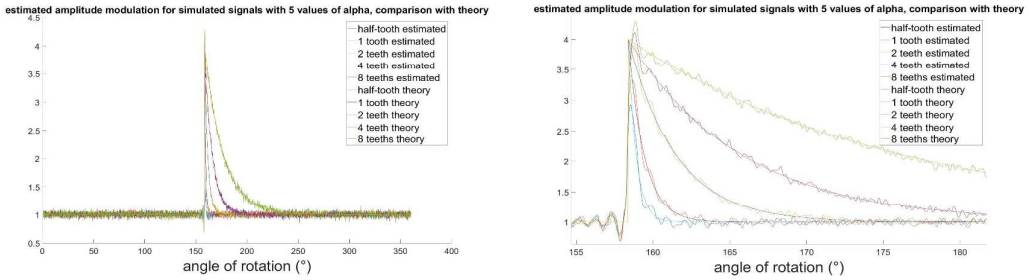

Figure 6: Theoretical and estimated $AM_h(t)$ for different damping factors, with a amplitude shock of 3 (left) and zoom on the shock instant (right).

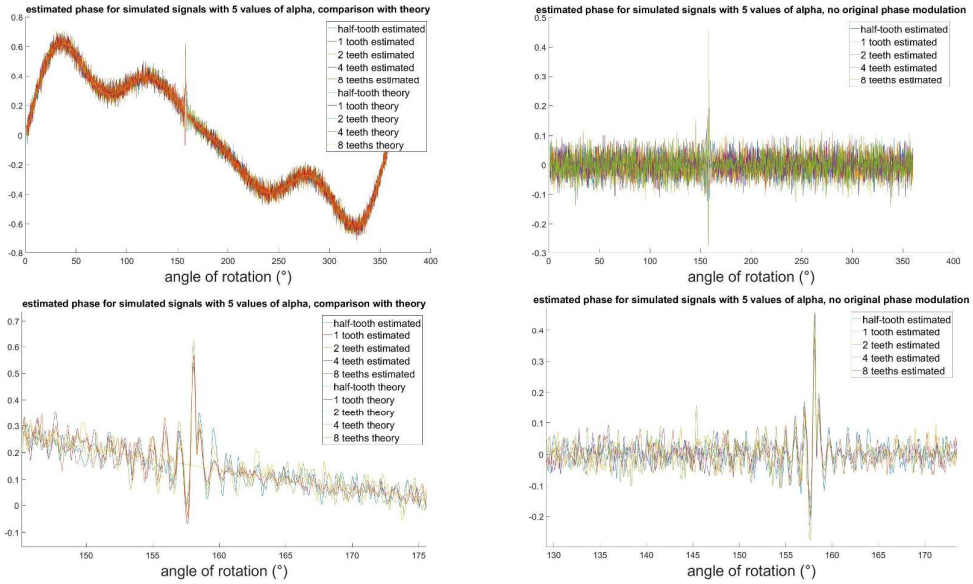

Figure 7: Estimated $PM_h(t)$ with different damping factors (top) and zoom on the shock time (bottom). On the left, $PM_h(t)$ with K=4, c=5. On the right, no $PM_h(t)$.

Table 1. MQE of $AM_h(t)$ and $PM_h(t)$ with various $PM_h(t)$ in the "friendly" case

	Theoretical $PM_h(t)$	Damping factor				
		½ tooth	1tooth	2 teeth	4 teeth	8 teeth
MQE of $AM_h(t)$	No PM	0.0017	0.0017	0.0017	0.0017	0.0022
	K=1 c=1	0.0021	0.0021	0.0024	0.0025	0.0027
	K=4 c=20	0.0025	0.0026	0.0027	0.0028	0.0031
MQE of $PM_h(t)$	No PM	0.0009	0.0010	0.0011	0.0011	0.0014
	K=1 c=1	0.0011	0.0011	0.0012	0.0012	0.0014
	K=4 c=20	0.0013	0.0012	0.0012	0.0013	0.0015

As shown on **Figure 6** and **Figure 7**, the demodulation is very efficient in this simplified case. The estimated $AM_h(t)$ and $PM_h(t)$ are very close to the original one, whatever the simulated PM_h. In order to evaluate the efficiency of the demodulation, the theoretical and estimated values were compared in Table 1 using the mean quadratic error (MQE).
All the values are very low, showing the efficiency of demodulation in this simplified case (only one mesh frequency, no interference in the demodulation caused by the other harmonics, and very large demodulation band). However, while this indicator reflects well the overall precision of the demodulation, it is enough. Indeed, **Figure 6** shows that both shocks are not correctly estimated compared to the theoretical ones. Thus, two indicators have been added: the shock amplitude error (SAE) and the shock position error (SPE). Let us denote A_s the shock amplitude, $\hat{A}_s$ its estimation, while $\hat{\theta}^{\zeta}$ denotes the estimation of the shock angular position $\theta^{\zeta} = f^{gear}\, t^{\zeta}/360$ over one gear rotation. So, SAE and SAP are defined by

$$SAE = \frac{|A_s - \widehat{A_s}|}{A_s} * 100 \text{ and } SPE = \left|\theta^{\zeta} - \widehat{\theta^{\zeta}}\right| \text{..} \quad \text{.....(8)}$$

Table 2: Errors of the estimated shock in the "friendly" case

	Indicator in %	Damping factor				
		½ tooth	1tooth	2 teeth	4 teeth	8 teeth
$AM_h(t)$ & no $PM_h(t)$	SAE	26.85	16.79	2.61	2.77	7.22
	SPE	0.14	0.16	0.44	0.41	0.47

Thus, despite being in a simplified case, Table 2 raises 3 problems:

- The shock amplitude is not correctly estimated for the shorter shocks (half-tooth and one tooth). The shorter the shock, the bigger the error is. This is confirmed by the SAE values, which goes up to 26.85% for the shortest shock.
- The estimated shock position is not accurate, even if the error is small compared to the tooth width (<0.5°).
- On Figure 7, the estimated $PM_h(t)$ shows a small shock at the same position as in $AM_h(t)$, albeit with a less amplitude, even where no $PM_h(t)$ was present in the simulated signal. This shows that the $PM_h(t)$ is influenced by $AM_h(t)$.

7.2. Demodulation in a realistic case

7.2.1. *Demodulation problem with real GOTIX signals*

The simulated signals have now every harmonics present, as in Equation (2). The analysis of a GOTIX signal spectrum with the AStrion-H, the harmonic and sideband classification module, shows that the predominant gearbox harmonics are surrounded by sidebands at the frequency of the input and output shaft. In order to simplify, only the sidebands from the input shaft have been included in the simulated signals.

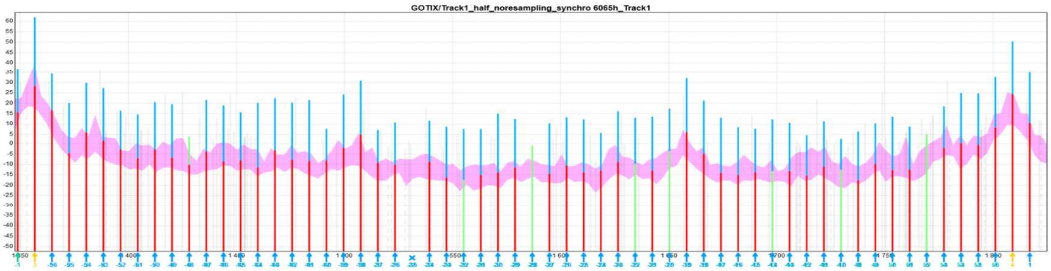

Figure 8: Sidebands detected by AStrion-H around H_3 and H_4 in a GOTIX signal.

The biggest drawback when demodulating around a gear mesh harmonic is that the meshing frequency is a multiple of the shaft rotation frequency. Thus, the sidebands around a mesh harmonic $H_n = nf^{mesh}$ are influenced by the sidebands of every other harmonics. It is tricky to determine which part of the sideband value is coming from H_n, and which part is coming from H_{n+1}. The same peaks will be classified by AStrion-H as sidebands around H_n and H_{n+1}. See Figure 8. Practically, this reduces drastically the number of sidebands usable for demodulation. Since GOTIX have 57 teeth on the gear, 57 sidebands are between each harmonic. The demodulation will be performed on half that number, thus between sidebands [-28 28] instead of the whole spectrum.
As the higher in amplitude, the 3rd harmonic has been chosen for the demodulation. The band of demodulation is thus [1131 1574] Hz. It is important to notice that an efficient multirate filter is applied to the signal in order to reach this band. That explains in particular why, on the following figures, there is much less high frequency noise.

7.2.2. *Comparison model-GOTIX for the amplitude modulation*

In this part, we will evaluate the effect of the shock duration on the demodulation process. Compared to **Figure 6**, the estimated $AM_h(t)$ in Figure 9 is less accurate in amplitude and the peak shape is rounder. This is confirmed by the MQE values in Table 3 showing values in this less friendly case around a hundred times higher than in table 1.

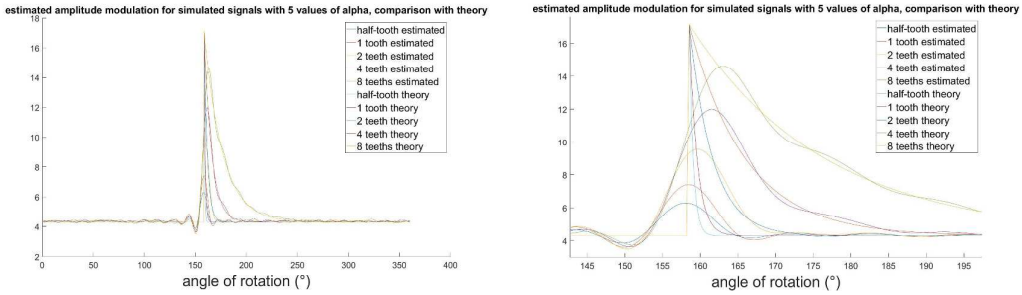

Figure 9: Theoretical and estimated $AM_h(t)$ for different damping factors, with a shock of amplitude 3 (left) and zoom on the shock time (right).

But the most problematic parts are actually the errors in the estimation of the shock amplitude and position. Table 4 shows that the error in the estimation of the shock amplitude can be very important, above 60%, especially for shorter shocks. In the contrary, the longer the shock is, the more important the error in the estimation of its position is. In GOTIX, the angle between 2 consecutive teeth is 6.3°. Thus, an error of 4° can induce diagnosis error in the defect tooth location. Furthermore, 2 different

defaults can have the same demodulation shape. As an example, a short shock with high amplitude, and a longer shock with lower amplitude can be difficult to distinguish.

Table 3. MQE of $AM_h(t)$ with various $PM_h(t)$ in the realistic case

	Theoretical $PM_h(t)$	Damping factor				
		½ tooth	1 tooth	2 teeth	4 teeth	8 teeth
MQE of $AM_h(t)$	No PM	0.1827	0.2327	0.3090	0.3188	0.3098
	K=1 c=1	0.1981	0.2523	0.3207	0.3237	0.3215
	K=4 c=20	0.2134	0.2692	0.3269	0.3359	0.3319

Table 4. Errors of the estimated shock in the realistic case

	Indicator in %	Damping factor				
		½ tooth	1tooth	2 teeth	4 teeth	8 teeth
$AM_h(t)$ & no $PM_h(t)$	SAE	63.30	56.82	44.29	30.14	14.79
	SPE	0.33	0	1.00	3.00	4.34

7.2.3. *Comparison model-GOTIX for the phase modulation*

As in the "friendly" case, $PM_h(t)$ is influenced by the shock in $AM_h(t)$, even when no $PM_h(t)$ is originally present. Compared to the previous case, this shock in $PM_h(t)$ is lower and larger due to the reduction of the demodulation band. Interestingly, the MQE shown in Table 5 are even lower in this case. This is probably due to the multirate filtering removing the high frequency noise present in the "friendly" case. It is enough to compensate the effect of the band reduction, contrary to $AM_h(t)$.

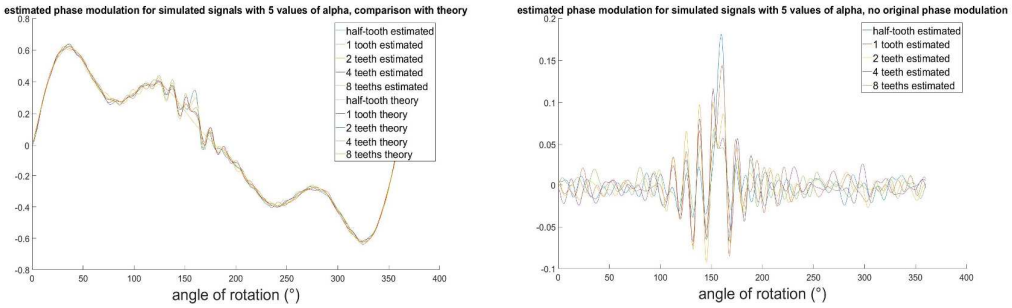

Figure 10: Theoretical ad estimated $PM_h(t)$ for different damping factors. On the left, $PM_h(t)$ K=4, c=5. On the right, no $PM_h(t)$

Table 5. MQE of $PM_h(t)$ with various $PM_h(t)$ in the realistic case

	Theoretical $PM_h(t)$	Damping factor				
		½ tooth	1tooth	2 teeth	4 teeth	8 teeth
MQE of $PM_h(t)$	No PM	0.0011	0.0010	0.0009	0.0005	0.0004
	K=1 c=1	0.0008	0.0007	0.0007	0.0006	0.0003
	K=4 c=20	0.0012	0.0013	0.0012	0.0007	0.0005

7.3. Explanations about the demodulation errors

There are mainly 2 reasons explaining the errors between theoretical and estimated $AM_h(t)$ and $PM_h(t)$, the filtering and the non-respect of the Bedrosian condition.

7.3.1. *Filtering problem*

As explained in part 7.2.1, the configuration of gearing systems compels the filtering to be applied on restricted bands. In the case of the shock model, the full spectrum is very large band. Thus, reducing this band removes the high frequencies of the shock. This is what mainly explains the rounding of the estimated shock, as well as the decrease in amplitude and the position shift observed.

However, since the original $PM_h(t)$ was at most a sum of 4 sines, its frequency range was very limited and mostly unaffected by the reduction of the band. Thus, in this case, the demodulation was very efficient to estimate the phase. However, while it has not been studied here, the demodulation of a quick phase variation, in the case of a missing tooth for example, would probably suffer the same limitations.

7.3.2. *Respect of the Bedrosian condition*

When applying the Hilbert transform, the Bedrosian constraints are respected only if the spectral support of $AM_h(t)$ denoted as B_M and the spectral support of $\sin(2\pi h f^{mesh} t + PM_h(t))$ denoted as B_Φ are disjointed. However, in the case of the shock function, B_M is theoretically infinite, and for $PM_h(t)$ equal a sum of sines, B_Φ is also infinite. For the purpose of this study, in order to understand the effect of the length of the shock, it is considered that the boundaries of B_M and B_Φ are defined for 98% of the energy. The 3rd GOTIX harmonic f^{mesh} used for the demodulation is at 1350Hz. Thus, according to Table 6, only the 8 tooth case respect the Bedrosian condition, if B_Φ is below 1260Hz.

Table 6. B_M and B_Φ for different $AM_h(t)$ (up) and for different $PM_h(t)$ (down)

$AM_h(t)$ Length of shock	½ tooth	1 tooth	2 teeth	4 teeth	8 teeth
B_M (Hz)	10449	8440	4145	1827	720

$PM_h(t)$	No PM	K=1 c=1	K=1 c=20	K=4 c=1	K=4 c=20
B_Φ (Hz)	0	15.8	332.2	0	47.5

As a reminder, the amplitudes of the 4 sines correspond to a healthy state of GOTIX, thus the values of these sines are low (<0.3). This explains the obtained bandwidths. Thus, the Bedrosian condition is less respected for K=1 and c=20, with a half-tooth shock. The study of the estimated $PM_h(t)$ revealed that it is influenced by the shock in $AM_h(t)$. This influence can be estimated by the maximum of the error between the estimated and theoretical one, because this maximum is always due to the shock.

Table 7: Maximum of the error of $PM_h(t)$

Length of shock	½ tooth	1tooth	2 teeth	4 teeth	8 teeth
No PM	0.18	0.14	0.10	0.11	0.07
K=1 c=1	0.23	0.19	0.14	0.09	0.07
K=1 c=20	0.47	0.51	0.46	0.40	0.38
K=4 c=1	0.19	0.15	0.11	0.09	0.06
K=4 c=20	0.23	0.20	0.17	0.11	0.06

Table 7 shows that the less the Bedrosian condition is respected, the more the estimated $PM_h(t)$ is influenced. Thus this condition is responsible for this influence. However, as shown by the MQE values of the estimated $PM_h(t)$, this influence is still limited compared with the influence of the filtering on $AM_h(t)$, $PM_h(t)$ is well estimated.

Finally, a non-realistic case is studied with a very strong $PM_h(t)$ defined as a sum of 4 sines with amplitudes of *[1 0.8 0.6 0.4]* and *c=20*. The corresponding bandwidth as previously defined is now 910 Hz. **Figure 11** shows that both estimated $AM_h(t)$ and $PM_h(t)$ are strongly disturbed.

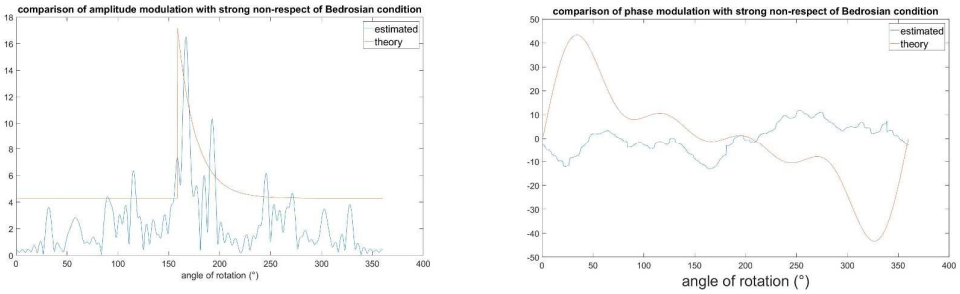

Figure 11: Comparison between theoretical and estimated $AM_h(t)$ (left) and $PM_h(t)$ (right) in the case of a strong non-respect of the Bedrosian condition.

8. Conclusions

To better understand the constraints of the demodulation process by Hilbert transform for the analysis of signals in context of system surveillance, this paper has proposed an analysis interpretation of both measured signals and signal models to highlight the limits of the method. Models of amplitude and phase modulation in the presence of a default on the gear have been proposed and validated by comparison with real measured signals. Future studies should improve the shock model, adding more shocks of various amplitudes to simulate each tooth, and include realistic models for phase problems, such as phase lag.

While the filtering on too-narrow bandwidth cannot be prevented, especially in the case of meshing systems, due to mechanical constraints, it is important to consider its effects in the diagnosis. However, it is possible to limit or prevent the effects of the Bedrosian condition. It is obvious that the compliance with Bedrosian constraints is less and less possible when demodulating in low frequency bands. It is thus preferable to demodulate higher harmonics, but the overall energy of the sidebands available has to be taken into account. The results will be a help for a further improvement of the method and most importantly for an optimal configuration of the demodulation process in the automatic data-driven AStrion tool. Further work should focus on the magnitude of the distortion in relation with both the bandwidth and the amplitude of the respective spectrums, and define the acceptability of this distortion for the diagnosis.

Finally, the monitoring of the evolution of these demodulations over a default dataset, possible with the AStrion software, will provide precious information on the efficiency of this technic on diagnosis.

Appendix. GOTIX test bench

Driving three-phase asynchronous motor Leroy-Somer P280 S-8, 55 kW. Braking DC generator Leroy-Somer 54.3 kW, commanded by a Leroy-Somer DMV 2342 inverter. The motor is powered either by 340V 50Hz AC or Altivar 66 inverter. Parallel straight teeth in case-hardened steel.

Tooth number, Gear $Z_g = 57$, Pinion $Z_p = 15$, $RPM(gear)=474rpm$

OROS acquisition system, sampling frequency $25.6\,KHz$, data length 10 s**,** 18 synchronous channels (6 accelerometers, 3 phase current & voltage measurement, 1 torquemeter, 1 tachometer and 2 optical encoders with top-tour.

Further http://www.gipsa-lab.grenoble-inp.fr/projet/gotix/presentation.html

References

1. N. Martin, C. Mailhes, 'Automatic Data-Driven Spectral Analysis Based on a Multi-Estimator Approach', Signal processing, Vol. 146, pp 112-125, May 2018.
2. T. Gerber, N. Martin, C. Mailhes, 'Time-frequency Tracking of Spectral Structures Estimated by a Data-driven Method', IEEE Trans. on Industrial Electronics, Special Session, Vol. 52, Issue 10, pp 6616-6626, October 2015.
3. N. Martin, Invited Keynote Address, 'KAStrion project: a new concept for the condition monitoring of wind turbines', CM-MFPT 2015,, UK, 9-11 June 2015.
4. Z.-Y. Li, T. Gerber, M. Firla, P. Bellemain, N. Martin, C. Mailhes, 'AStrion strategy: from acquisition to diagnosis. Application to wind turbine monitoring'. International Journal of Condition Monitoring, Vol. 6, No 2, pp 47-54, June 2016.
5. X. Laval, G. Song, Z.-Y. Li, P. Bellemain, M. Lefray, N. Martin, A. Lebranchu, C. Mailhes, Invited Keynote Address, 'AStrion assets for the detection of a main bearing failure in an onshore wind turbine', CM-MFPT 2016, France, 10-12 October 2016.
6. M. Eltabach, S. Sieg-Zieba, G. Song, Z.-Y. Li, P. Bellemain, N. Martin, 'Vibration condition monitoring in a paper industrial plant: Supreme project', CM 2016 and MFPT 2016. Paris, France, 10-12 October 2016.
7. M. Firla, Z.-Y. Li, N. Martin, C. Pachaud, T. Barszcz, 'Automatic Characteristic Frequency Association and All-Sidebands Demodulation for Detection of a Bearing Fault of a Wind Turbine Test Rig', MSSP, Vol. 80, pp 335-348, December 2016.
8. N. Martin, P. Jaussaud, F. Combet, 'Close shocks detection using time-frequency Prony Modelling', MSSP, Vol. 18, n°2, pp 235-261, March 2004.
9. R.B. Randall, 'Vibration-based Condition Monitoring', J. Wiley & Sons Ed., 2011.
10. P.D. McFadden, 'Detecting Fatigue Cracks in Gears by Amplitude and Phase Demodulation of the Meshing Vibration', Journal of Vibration, Acoustics, Stress, and Reliability in Design, Vol. 108, pp 165-170, April 1986.
11. J. Ma and C.J. Li, 'Gear Defect Detection through Model-Based Wideband Demodulation of Vibrations', MSSP, 10(5), pp 653-665, 1996.
12. C. Pachaud, T. Gerber, M. Firla, N. Martin, C. Mailhes, 'Consequences of non-respect of the Bedrosian theorem when demodulating'. CM-MFPT 2013, Cracovie, Poland, June 18-20 2013.
13. D.Abboud, J. Antoni, S. Sieg-Zieba, M. Eltabach, 'Envelope analysis of rotating machine vibrations in variable speed conditions: A comprehensible treatment', MSSP, Vol. 84, n°2, pp 200-226, 2017.
14. G. Song, Z.-Y. Li, P. Bellemain, N. Martin, C. Mailhes, 'AStrion data validation of non-stationary wind turbine signals', CM-MFPT 2015, UK, June 9-11, 2015.